American Mineralogist, Volume 106, pages 1844–1851, 2021

Johnkoivulaite, $Cs(Be_2B)Mg_2Si_6O_{18}$, a new mineral of the beryl group from the gem deposits of Mogok, Myanmar

Aaron C. Palke[1,*], Lawrence M. Henling[2], Chi Ma[3,†], George R. Rossman[3], Ziyin Sun[1], Nathan Renfro[1], Anthony R. Kampf[4,‡], Kyaw Thu[5], Nay Myo[6], Patcharee Wongrawang[7], and Vararut Weeramonkhonlert[7]

[1]Gemological Institute of America, Carlsbad, California 92008, U.S.A.
[2]Beckman Institute, California Institute of Technology, Pasadena, California 91125, U.S.A.
[3]Division of Geological and Planetary Sciences, California Institute of Technology, Pasadena, California 91125, U.S.A.
[4]Mineral Sciences Department, Natural History Museum of Los Angeles County, Los Angeles, California 90007, U.S.A.
[5]S Gemmological Institute, Yangon 11201, Myanmar
[6]Greatland Gems and Jewelry, Mogok 11101, Myanmar
[7]Gemological Institute of America, Bangkok 10500, Thailand

Abstract

A new mineral of the beryl group, johnkoivulaite, $Cs(Be_2B)Mg_2Si_6O_{18}$, was recovered from the gem gravels in the Pein Pyit area of the Mogok region in Myanmar. Thus far, only a single crystal has been identified. It has dimensions of about 5.8 × 5.7 × 5.5 mm. This specimen has an irregular shape but still has discernible crystal form with geometric growth patterns observed on the crystal faces. The crystal of johnkoivulaite is grayish-violet in color and strongly pleochroic, going from nearly colorless with E⊥**c** to dark bluish-violet with E||**c**. Johnkoivulaite has a Mohs hardness of about 7½ and a measured density of 3.01(10) g/cm^3. It is uniaxial (–) with ω = 1.607(1) and ε = 1.605(1) (white light). Electron microprobe analyses gave the empirical formula of $(Cs_{0.85}K_{0.10}Na_{0.01})(Be_{1.88}B_{1.12})(Mg_{1.66}Fe_{0.27}Mn_{0.01}Al_{0.05})(Si_{5.98})O_{18}$ with Be calculated by stoichiometry and confirmed by LA-ICP-MS measurements. Johnkoivulaite is hexagonal, *P*6/*mmc* (no. 192) with $a = 9.469(2)$, $c = 9.033(2)$ Å, $V = 701.5(3)$ Å^3, and $Z = 2$. Johnkoivulaite is isostructural with beryl and exhibits partial substitution of B for Be at the distorted tetrahedral site, Mg for Al at the octahedral site, and Cs in the channel sites within the stacked Si_6O_{18} rings. This substitution can be written as $(CsMg_2B)(\square Al_2Be)_{-1}$. Johnkoivulaite, the seventh member of the beryl group, is named in honor of gemologist John Koivula in recognition of his contributions to mineralogy and gemology.

Keywords: Beryl group, new mineral, gemology, johnkoivulaite, Mogok, Myanmar

Introduction

Mogok, Myanmar, is one of the most geologically diverse locales in the world. Not only does Mogok produce some of the finest quality rubies, but it is also the source of some of the finest blue sapphire, spinel, peridot, gem feldspar, and numerous other gems. The geological processes that created the gemstone deposits in Mogok also created an assortment of rare minerals found nowhere else in the world, such as painite and kyawthuite. Additionally, ~50 km northeast of Mogok, near the Momeik township, another rare mineral, avdeevite, of the beryl group was recently found, further adding to the geological diversity of this region. Another rare member of the beryl family, pezzottaite, has also been found in this region, being found in the Molo quarter of the Momeik township and east of Let Pan Hla, Pyin Gyi Taung between the cities of Mandalay and Mogok.

In this contribution, we describe another rare mineral unique to Mogok, johnkoivulaite, also a member of the beryl group. The new mineral was named in recognition of the lifetime work of John Koivula of the Gemological Institute of America and his many achievements and contributions to the fields of mineralogy and gemology. The new mineral and name were approved by the IMA Commission on New Minerals, Nomenclature and Classification on September 6, 2019, under the number 2019-046. The holotype specimen of johnkoivulaite is permanently deposited in the collection of the Gemological Institute of America Museum under its catalog number 41653, and the co-type consisting of several tiny fragments from the holotype is deposited in the collections of the Natural History Museum of Los Angeles County, California, U.S.A., under catalog number 75133.

Location and geological background

The Mogok gem deposits are found within the Mogok metamorphic belt stretching approximately north-south from southern Myanmar in the Andaman Sea up into northern Myanmar near the eastern Himalayan syntaxis (Searle et al. 2007). The Mogok metamorphic belt was produced by compressive and transtensional deformation during the Himalayan orogeny in the late

* E-mail: apalke@gia.edu
† Orcid 0000-0002-1828-7033
‡ Orcid 0000-0001-8084-2563

0003-004X/21/0011–1844$05.00/DOI: https://doi.org/10.2138/am-2021-7785

Cretaceous to the Cenozoic time. The rubies and spinels in the Mogok region are hosted in relatively pure marbles produced by this metamorphic event, whereas blue sapphires and many of the other gems are more closely associated with igneous activity in the area, especially syenitic pegmatites that are often found near the contacts between gneisses or marbles with large bodies of syenites or other alkaline intrusives (e.g., Thu 2007). There is also a famous peridot mine near the north of the Mogok region related to hydrothermal alteration of an ophiolitic body emplaced during the Himalayan orogeny. Unfortunately for the geologists interested in the finer details of the geological genesis of gem deposits, most of the important gem mines in the Mogok region are secondary deposits except for some of the marble-hosted ruby/spinel mines. In these secondary deposits, the precious gems have weathered out of their original host rock and are washed downstream or downslope. As gem corundum and many other gem materials are quite dense, they can get sequestered in gravel deposits in these secondary deposits.

This is also the case for the new mineral, which was produced from an alluvial mining operation in the Pein Pyit area (GPS coordinates: 22°58′33.92″N, 96°33′41.75″E) of the Mogok region of Myanmar. Pein Pyit is a historic mining site in the Mogok region, with most mining taking place in secondary alluvial deposits. Ruby and spinel are the primary targets of mining activity, but sapphires, tourmaline, topaz, and gem feldspar are also produced in the Pein Pyit area. The new mineral is a relatively hard and refractory material that weathered out of the metamorphic and/or igneous rocks in the Pein Pyit area and survived to be interred in a secondary alluvial deposit. It is unclear what the original host rock would have been, but the dominant geological formations in the immediate area are marbles, which are intruded by granites and syenites with associated pegmatites of similar composition. The single sample of the new mineral studied here was recovered as a single crystal, and there is little direct evidence of coexisting mineral assemblages. However, notable gem minerals also found in the Pein Pyit gem gravels include danburite, poudretteite, hackmanite, orthoclase, scapolite, apatite, and muscovite, which indicate the importance of pegmatites in this area.

The stone was originally obtained by Nay Myo, a local gem dealer. Nay Myo recognized that the stone's basic properties did not match any of the typical gem species expected from this area. He suspected this might be something new and so he submitted the stone to the Identification Laboratory of the Gemological Institute of America first in Bangkok, Thailand, and then again in Carlsbad, California, U.S.A.

Materials and methods

LA-ICP-MS chemical analyses

Laser ablation-inductively coupled plasma-mass spectrometry (LA-ICP-MS) was used at the Gemological Institute of America in Carlsbad, California, U.S.A. for chemical analysis of the new mineral using a Thermo-Fisher iCAP Qc ICP-MS, coupled with an Elemental Scientific NWR 213 laser ablation unit with a frequency-quintupled Nd:YAG laser (213 nm wavelength) running at 4 ns pulse width. Ablation was achieved using a 55 µm diameter laser spot size, a fluence (energy density) of approximately 10–12 J/cm^2, and a 20 Hz repetition rate. Argon was used as nebulizer gas (0.73 L/min), auxiliary gas (0.8 L/min), and cooling gas (14 L/min). Helium was used as the carrier gas at a flow rate of 0.8 L/min. Argon and helium gas flow, torch position, sampling depth, and lens voltage were optimized to achieve maximum sensitivity (counts per concentration) and low-oxide production rates (^{232}Th^{16}O/^{232}Th < 1%). Ablated material was vaporized, atomized, and ionized by an argon plasma using a power of 1550 W. The dwell time of each isotope measured was 0.01 s except ^{28}Si, which was measured for 0.005 s. The gas background was measured for 20 s, while the dwell time of each laser spot was 40 s. ^{29}Si was used as an internal standard with its initial value guessed with subsequent renormalization of the results to produce 100 wt% oxides. GSD-1G, GSE-1G (U.S. Geological Survey), and NIST 610 were used as external standards. Isotopes measured for the elements reported here include ^{9}Be, ^{11}B, ^{23}Na, ^{24}Mg, ^{27}Al, ^{29}Si ^{39}K, ^{55}Mn, ^{57}Fe, and ^{133}Cs. Other isotopes, including ^{7}Li were measured as well but were found at low concentrations (<1000 ppm) that would not affect the reporting of major elements contributing to the stoichiometry of this mineral.

Electron probe microanalysis (EPMA)

Accurate chemical analyses were obtained at the California Institute of Technology on a JEOL JXA-8200 electron microprobe. For all measured elements except B, 16 measurements were made using analytical conditions of 15 kV accelerating voltage, 25 nA beam current, and a defocused beam diameter of 10 µm. Separate B measurements were made with EPMA with nine independent measurements using lower accelerating voltage of 10 kV, 30 nA, and a defocused beam diameter of 10 µm. Standards employed were danburite (B), albite (Na), synthetic forsterite (Mg), anorthite (Al, Si), microcline (K), synthetic tephroite (Mn), fayalite (Fe), and pollucite (Cs). (The danburite and pollucite standards were developed specifically for this project. The danburite was essentially the pure end-member, and the B_2O_3 concentration was determined by accurately measuring the CaO and SiO_2 concentrations and assuming a stoichiometric formula with B_2O_3 making up the difference between 100 wt% and the sum of the CaO and SiO_2 wt%. The Cs_2O value for the pollucite standard was determined in a similar way by accurately measuring K_2O, Na_2O, Al_2O_3, and SiO_2 wt% values and ensuring charge balance and a stoichiometric pollucite formula by forcing atoms of Al to equal the sum of K+Na+Cs. The total of the pollucite standard came out at 99.3 wt%.) Raw X-ray intensities were corrected for matrix effects with the CITZAF procedure (Armstrong 1995). Analytical precision is estimated to be ±1% relative for the major elements and ±5% for the minor elements.

Raman spectroscopy

Raman spectra were obtained using a Renishaw inVia Raman microscope system with a Modu-Laser Stellar-REN Ar-ion laser producing highly polarized light at 514 nm and collected at a nominal resolution of 3 cm^{-1} in the 2000–200 cm^{-1} range. A 5× objective lens was used to focus the laser on the surface of the sample.

Infrared spectroscopy

Fourier-transform infrared (FTIR) spectroscopy was performed using a Thermo-Nicolet 6700 FTIR spectrometer equipped with an XT-KBr beam splitter and a mercury-cadmium-telluride (MCT) detector operating with a 4× beam condenser accessory. The resolution was set at 2 cm^{-1} with 1.928 cm^{-1} data spacing. The spectrum was averaged from 200 acquisitions.

UV-Vis spectroscopy

UV-Vis spectra were recorded with a PerkinElmer Lambda 950 in the range of 190–1100 nm with a 1 nm spectral resolution and a scan speed of 400 nm/min.

Single-crystal X-ray diffraction

A small fragment broken off the main crystal was mounted on a polyimide MiTeGen loop with STP Oil Treatment and placed in the 100 K nitrogen stream of an Oxford Cryosystems 700 Series Cryostream Cooler. X-ray data were collected with a Bruker AXS D8 KAPPA APEX II diffractometer (Siemens KFF Mo 2K-90 fine-focus sealed tube with Mo$K\alpha$ = 0.71073 Å operated at 50 kV and 30 mA; TRIUMPH graphite monochromator; PHOTON 100 CMOS area detector with a resolution of 10.24 pixels/mm). A combination of 1526 ω- and φ-scans spanning 5° to 89° in 2θ were collected with a 1° width and collection times ranging from 5 to 25 s. All diffractometer manipulations, including data collection, integration, and scaling were carried out using the Bruker APEX3 software (Bruker 2012). A face-indexed absorption correction with µ refined was followed by a multiscan correction with an additional spherical absorption correction with $\mu \cdot r = 1.0$ using SADABS (Bruker 2001). The space group was determined and the structure solved by intrinsic phasing using XT. Refinement was full-matrix least squares on F^2 using XL. All atoms were refined using anisotropic displacement parameters. Full crystallographic data are included in the crystallographic information framework (CIF[1]) file, available as Online Material[1].

Powder X-ray diffraction

Powder X–ray studies were done using a Rigaku R-Axis Rapid II curved imaging plate microdiffractometer with monochromatized Mo*K*α radiation (λ = 0.71075 Å). A Gandolfi-like motion on the φ and ω axes was used to randomize the samples and observed *d*-values and intensities were derived by profile fitting using JADE Pro software (Materials Data, Inc.). The cell parameters were refined from the powder data using JADE Pro with whole pattern fitting.

Results

Physical and optical properties of johnkoivulaite

The single crystal of johnkoivulaite studied here occurs as an irregularly shaped crystal with dimensions of 5.8 × 5.7 × 5.5 mm and weighing 0.234 g (Fig. 1). Despite the lack of any well-defined crystal form, the specimen has not been abraded by alluvial transport but appears to have discernible crystal faces with geometric growth patterns observed on the surfaces. In fact, there does seem to be a somewhat prismatic appearance to the crystal, with what appears to be a basal pinacoid terminating one end. However, whatever crystal form was present initially seems to be obfuscated by later etching along the surfaces (Fig. 2) and fracturing and breakage along one side.

Johnkoivulaite has a hardness of about 7½, a white streak, vitreous luster, and breaks in a brittle fashion. There is no observable cleavage or parting, and the stone exhibits conchoidal fracture. The density is 3.01(10) g/cm^3 measured by weighing in air and again suspended in water. Note that the estimated error is given by variations in measured density by repeat measurements. Additionally, the density here is likely measured too low given the irregular shape of the crystal and the possibility that small gas bubbles were trapped in small cracks and cavities on the stone's surface, despite our best efforts to remove such features during measurement. The stone is non-fluorescent in longwave (~360 nm) or shortwave (~254 nm) standard UV lamps. Johnkoivulaite has a uniaxial optic character as determined by observation of its optic figure in a gemological polariscope. A small chip was removed from the sample, and a uniaxial negative interference figure was observed on a petrographic microscope. The indices of refraction were determined to be ω = 1.607(1) and ε = 1.605(1) using standard refractive index liquids.

The holotype crystal of johnkoivulaite is slightly grayish violet when viewed in daylight. Of particular note is the stone's extreme pleochroism going from nearly colorless (with the polarized electric vector of the light E⊥**c**, or as the o-ray) to dark bluish-violet (with the polarized electric vector E||**c**, or as the e-ray) when observed in polarized light (Fig. 3). However, no pleochroism was observable in the small crystal fragments used for the optical measurements.

Observations of the stone's inclusions, unfortunately, did not shed light on the geological origin of the mineral. The only internal features that could be discerned were linear tubes that appear to be crystallographically aligned with the c-axis, which seem to have been infiltrated by fluids, which precipitated what is likely to be iron-oxide minerals. These tubes are interpreted to be either growth tubes or etch tubes (Fig. 4), which are common inclusions in beryl and other pegmatite minerals (Gübelin and Koivula 1986).

Raman spectroscopic data

When the new mineral was first submitted to the Identification lab at the Gemological Institute of America, its measured properties did not match any obvious known mineral species. Therefore, the first additional piece of evidence sought was Raman spectroscopy that can be a very powerful fingerprinting tool for mineral species when a robust reference database is available. The Raman spectrum of johnkoivulaite is shown in Figure 5. When referenced against the RRUFF database, there were no complete matches. The closest match, however, was with beryl. The dominant peaks in the Raman spectrum of johnkoivulaite occur at 1084, 691, 623, 405, 260, and 226 cm^{-1}, which generally match with the dominant bands in beryl at 1067, 683, 396, and 323 cm^{-1} (from the RRUFF database, Lafuente et al. 2015). Figure 5 shows the polarized Raman spectra of the polarized component of the light E||**c** and E⊥**c**. For end-member beryl, there are a large number of peaks in the range of 100–1500 cm^{-1}, which previous workers have attributed to vibrations of the Si_6O_{18} rings, with or without involvement of neighboring BeO_4 and/or AlO_6 groups (Adams and Gardner 1974; Hagemann et al. 1990; Kim et al. 1995). The overall similarity between the Raman spectrum of johnkoivulaite and that of beryl suggests the Raman bands observed between 1100 and 100 cm^{-1} for johnkoivulaite are related to vibrational modes of the Si_6O_{18} rings potentially with the involvement of MgO_6 and BeO_4 or BO_4 groups. However, the

Figure 1. Photo of the single confirmed specimen of johnkoivulaite. Photo by Robert Weldon. ©GIA.

Figure 2. Photomicrograph of the surface of johnkoivulaite showing a slightly corroded pattern. Field of view 1.44 mm. Photomicrograph by Nathan Renfro. ©GIA.

more complex composition of johnkoivulaite precludes a deeper comparison and assignment of individual vibrational bands.

IR spectroscopic data

The FTIR spectrum of johnkoivulaite shows two strong absorption bands at 3589 and 3659 cm^{-1} (Fig. 6). These peaks correspond to molecular water in the channels of the crystal structure. Given the high-alkali content of johnkoivulaite and comparison with IR spectra of alkali-rich beryl, these peaks are likely equivalent to the type II water species seen in the IR spectra of alkali-rich beryl in which the water is associated with alkali ions contained in the channels (Aurisicchio et al. 1994).

UV-visible absorption spectroscopic data

The main absorption feature seen in the UV-Vis absorption spectrum is the broadband around 560 nm (Fig. 7). With the polarized component of the light E||**c** (or measuring the e-ray), this feature absorbs a significant portion of the green, yellow, and orange light passing through the stone while allowing much of the red and blue light to pass through, imparting a deep violet color with E||**c** polarized light (the e-ray). On the other hand, this feature nearly disappears with the polarized component of the light E⊥**c** (or measuring the o-ray absorption), and there is very little absorption of visible light. Another absorption feature observed is the band at about 850 nm in the near-IR, which does not change much with polarization of the light and does not significantly affect the color of this material. This absorption spectrum is similar to that seen for aquamarine (blue beryl); only the polarizable broad band around 560 nm is shifted down in energy in beryl to about 680 nm and most of the red light gets absorbed leading to a purer blue color. Aquamarine is also significantly pleochroic going from blue to nearly colorless due to this similar absorption feature (e.g., Palke and Hapeman 2019). The absorption feature in aquamarine is caused by Fe^{2+}-Fe^{3+} intervalence charge transfer (IVCT) (Fritsch and Rossman 1988). This Fe^{2+}-Fe^{3+} IVCT is likely the cause of the absorption band at 560 nm in johnkoivulaite. Note that a similar feature is seen as well in cordierite and is also attributed to Fe^{2+}-Fe^{3+} IVCT (Taran and Rossman 2001). Another explanation of this band at 560 nm in johnkoivulaite is the possible presence of Mn^{3+} as in red beryl. However, the polarization of Mn^{3+} behavior in beryl is not consistent with the polarization of the 560 nm band in johnkoivulaite (e.g., Nassau and Wood 1968; Fridrichová et al. 2018). Aquamarine also shows a similar near-IR, absorption band around 830 nm that has been ascribed to octahedrally coordinated Fe^{2+} (Taran and Rossman 2001), which suggests the 850 nm band in johnkoivulaite has a similar origin. The relatively narrow and weak absorption bands sometimes seen in aquamarine at around 370 and 430 nm related to octahedral Fe^{3+} are not observed in johnkoivulaite.

Chemical composition

The chemical composition of johnkoivulaite was first investigated using LA-ICP-MS. While not generally considered to be as quantitatively accurate as EPMA for major elements, LA-ICP-MS has the advantage of being able to measure most of the elements in a single analysis as well as having much greater sensitivity than EPMA, allowing trace elements to be readily detected. The major elements measured by LA-ICP-MS were Be, B, Mg, Si, Fe, and Cs. Additionally, Na, Al, K, and Mn were detected as minor elements while only traces of other elements were measured (Table 1).

Using the preliminary chemical data from LA-ICP-MS, we were able to take a more focused approach to the EPMA analysis.

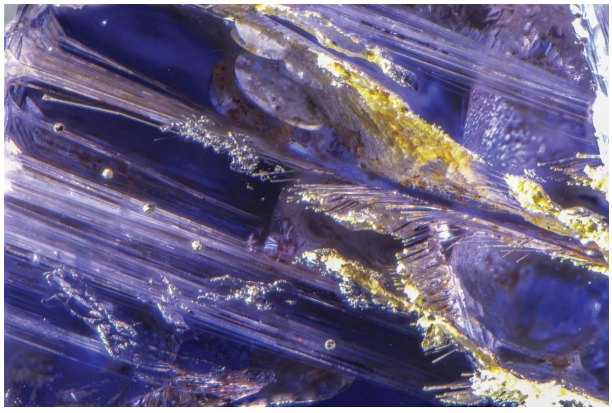

Figure 4. Photomicrograph of the inclusions within johnkoivulaite which include growth tubes (or etch tubes), which are crystallographically aligned to the johnkoivulaite host. Field of view 4.12 mm. Photomicrograph by Nathan Renfro. ©GIA.

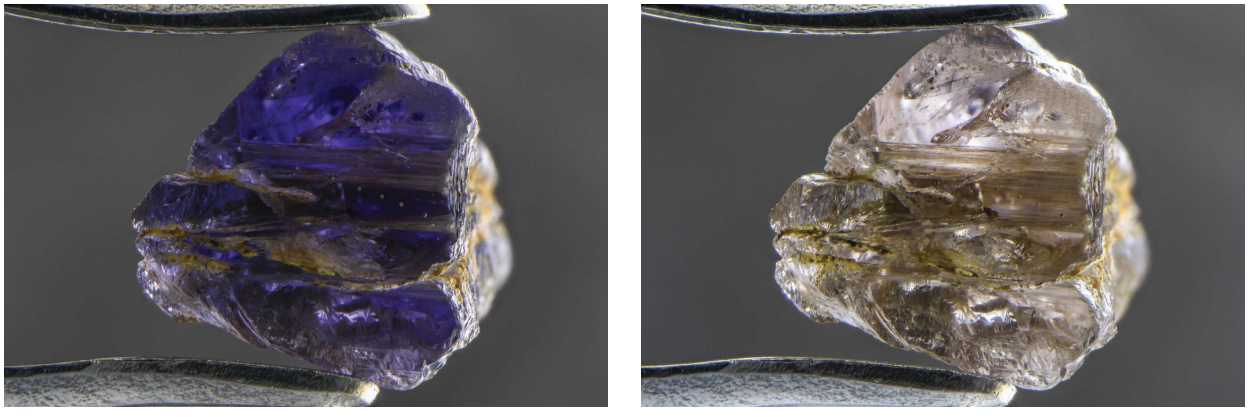

Figure 3. Photomicrograph of johnkoivulaite with light polarized parallel to the e-ray (**left**) and o-ray (**right**). Fields of view 10.05 mm. ©GIA.

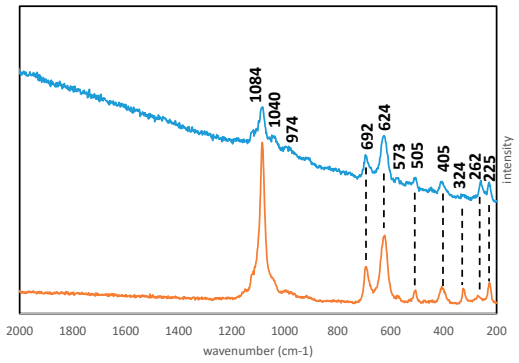

Figure 5. Raman spectra of johnkoivulaite in both E||**c** (blue) and E⊥**c** (orange) polarization.

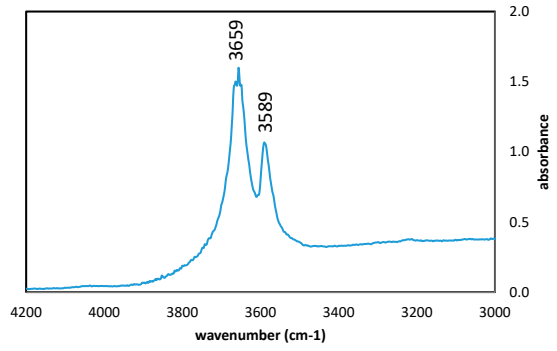

Figure 6. FTIR spectrum of johnkoivulaite.

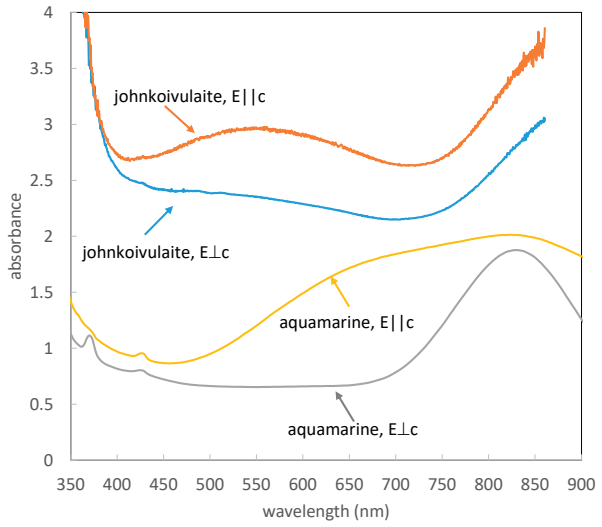

Figure 7. UV-Vis spectrum of johnkoivulaite compared against that of deep blue aquamarine (beryl) from Nigeria (Palke and Hapeman 2019). Note that the spectra are offset vertically for the sake of comparison.

As discussed in the methods section, our EPMA analyses were able to measure all of the major and minor elements in johnkoivulaite except for Be, even though wavelength scans were employed in an attempt to make at least qualitative measurements of Be. Additionally, our B measurements were taken during a different EPMA session on different spots than the rest of the major and minor elements. The LA-ICP-MS analysis indicates that the only major element not detected by EPMA was Be. Given the data collected so far, which suggest the new mineral belongs to the beryl family, we can impose the constraints that there must be 18 O per formula, and we can assume that both Be and B would occupy the distorted tetrahedral site in a beryl group structure and that the sum of Be and B must equal 3. Using these constraints, the wt% BeO was calculated from this formula, with the resulting wt% oxide sum being 101.53 wt%. The results of EPMA measurements are given in Table 2. In general, the LA-ICP-MS analyses are in surprisingly good agreement with the EPMA measurements. Based on the EPMA measurements, the full empirical chemical formula of johnkoivulaite can be given as $(Cs_{0.85}K_{0.10}Na_{0.01})(Be_{1.88}B_{1.12})(Mg_{1.66}Fe_{0.27}Mn_{0.01}Al_{0.05})(Si_{5.98})O_{18}$ and the generalized ideal chemical formula is $Cs(Be_2B)Mg_2Si_6O_{18}$.

Table 1. LA-ICP-MS results (in wt%) measured for johnkoivulaite averaged over six spot analyses and renormalized to 100 wt% oxides

Constituent	Mean
BeO	9.58
B_2O_3	4.66
Na_2O	0.03
MgO	10.08
Al_2O_3	0.39
SiO_2	54.19
K_2O	0.70
MnO	0.11
FeO	3.04
Cs_2O	17.20
Total	99.98

Crystal structure of johnkoivulaite

A small fragment (0.18 × 0.33 × 0.47 mm) removed from the holotype specimen was used for the single-crystal X-ray structure analysis. Johnkoivulaite (as well as beryl) crystallizes in the hexagonal space group *P6/mmc* (no. 192), with $a = 9.469(2)$ Å, $c = 9.033(2)$ Å, $V = 701.5(3)$ Å^3, and $Z = 2$. The calculated densities of johnkoivulaite are 3.117 g/cm^3 using the empirical formula and 3.157 g/cm^3 with the ideal formula, which are in reasonably good agreement with the measured density of 3.01(10) g/cm^3.

The main structural units of johnkoivulaite are the Si_6O_{18} rings, which are stacked along the **c**-axis creating large channels into which the Cs atoms are stuffed at the 2*a* position in a site coordinated by 12 O atoms. While this site is vacant in the pure beryl structure, this is where Cs and other large alkali cations are

Table 2. Electron microprobe analytical data (in wt%) measured for johnkoivulaite

Constituent	Mean	Range	SD	Standard
BeO[a]	7.25			
B_2O_3	5.99	5.79–6.29	0.14	Danburite
Na_2O	0.04	0.01–0.08	0.02	Albite
MgO	10.34	10.24–10.43	0.06	Syn. forsterite
Al_2O_3	0.38	0.35–0.41	0.02	Anorthite
SiO_2	55.36	54.56–55.68	0.11	Anorthite
K_2O	0.71	0.69–0.73	0.01	Microcline
MnO	0.10	0.07–0.12	0.02	Syn. tephroite
FeO	2.98	2.92–3.04	0.04	Fayalite
Cs_2O	18.36	18.15–18.79	0.14	Pollucite
Total	101.51			

[a] Calculated to satisfy beryl-type formula with 18 O and Be+B = 3.

located in alkali-rich beryl (Brown and Mills 1986; Aurisicchio et al. 1988). The Si_6O_{18} rings are interlinked by distorted $(B,Be)O_4$ tetrahedra and MgO_6 octahedra.

With the chemical analyses described above as a starting basis, the site occupancies can be refined to give an empirical formula for this specimen of johnkoivulaite. Based on chemical analysis, the Cs site was refined as a mixture of Cs and K (0.81:0.19, site constrained to full occupancy); the Mg site as a mixture of Mg and Fe (1.72:0.29, site constrained to full occupancy); and the Be site as a mixture of Be and B (2.08:0.93, site constrained to full occupancy). The Be to B ratio is more unreliable than the statistics suggest due to the significant X-ray absorption by cesium compounded by the irregular shape of the sample. The minor constituents Na, Mn, and Al were not included in the model.

The atomic coordinates and displacement parameters for johnkoivulaite are given in Tables 3–4, and selected bond distances are given in Table 5. The structure of johnkoivulaite is illustrated in Figures 8 to 9.

A few small chips (~100–400 μm in size) were removed from the specimen of johnkoivulaite and gently crushed for powder X-ray diffraction. The powder XRD data was indexed using the structure derived from single-crystal XRD measurements and is reported in Table 6. Cell parameters refined from the powder XRD data are $a = 9.4657(11)$, $c = 9.0374(12)$ Å, and $V = 701.26(19)$ Å^3.

Relationship to other members of the beryl group

Relative to beryl, in ideal end-member johnkoivulaite, one of the three Be atoms in the distorted tetrahedral sites is replaced by B, all octahedral Al is replaced by Mg, Si occupies all the polymerized tetrahedral sites in the ring structures, and Cs sits within the channel sites at the 2*a* position. One of the major differences between johnkoivulaite and beryl is the addition of a discrete structural site for Cs^+ in johnkoivulaite. The addition of this cation in the channel is balanced by the substitution of Mg^{2+} for Al^{3+} in the octahedral site, as well as by B^{3+} replacing Be^{2+} in one of the three distorted tetrahedral sites; the substitution can be written as $(CsMg_2B)(\square Al_2Be)_{-1}$. This is similar to another member of the beryl group, pezzottaite $[Cs(Be_2Li)Al_2Si_6O_{18}]$, which also has a discrete structural site for Cs. The charge-balanced substitution between johnkoivulaite and pezzottaite can be written as $(Mg_2B)(Al_2Li)_{-1}$. The seven members of the beryl group are listed in Table 7.

Chemically, johnkoivulaite is similar to pezzottaite in which heterovalent substitutions occur for Be in the distorted tetrahedral site. However, johnkoivulaite is structurally distinct from pezzottaite in that both Be and B occupy the same structurally and symmetrically identical site in johnkoivulaite, whereas in pezzottaite this site is split, with Be and Li occupying structurally and symmetrically distinct sites. For this reason, johnkoivulaite maintains the higher symmetry space group of *P6*/*mcc* while pezzottaite has an ordered superstructure with lower symmetry trigonal space group of *R*3*c*. Johnkoivulaite is structurally more similar to Cs-rich beryl (Lambruschi et al. 2014).

Table 3. Atomic coordinates, equivalent isotropic displacement parameters (Å^2), and occupancies for johnkoivulaite

	x/*a*	*y*/*b*	*z*/*c*	U_{eq}	Occupancy
Cs	0	0	0.25	0.01208(3)	0.814(2)
K	0	0	0.25	0.01208(3)	0.186(2)
Si	0.62438(2)	0.72095(2)	0.5	0.00426(4)	1
Mg	0.33333	0.66667	0.75	0.00514(9)	0.857(3)
Fe	0.33333	0.66667	0.75	0.00514(9)	0.143(3)
O(1)	0.51928(4)	0.64492(4)	0.64773(4)	0.00978(6)	1
O(2)	0.78438(6)	0.70106(6)	0.5	0.01045(7)	1
Be	0.5	0.5	0.75	0.0049(3)	0.69(4)
B	0.5	0.5	0.75	0.0049(3)	0.31(4)

Table 4. Anisotropic displacement parameters (Å^2) for johnkoivulaite: the anisotropic displacement factor exponent takes the form: $-2\pi^2(h^2a^{\cdot 2}U_{11} + ... + 2hka{\cdot}b{\cdot}U_{12})$

	U_{11}	U_{22}	U_{33}	U_{23}	U_{13}	U_{12}
Cs	0.01390(4)	0.01390(4)	0.00844(4)	0	0	0.00695(2)
K	0.01390(4)	0.01390(4)	0.00844(4)	0	0	0.00695(2)
Si	0.00363(6)	0.00359(6)	0.00535(6)	0	0	0.00166(4)
Mg	0.00534(10)	0.00534(10)	0.00475(13)	0	0	0.00267(5)
Fe	0.00534(10)	0.00534(10)	0.00475(13)	0	0	0.00267(5)
O(1)	0.00956(11)	0.00724(10)	0.01092(11)	0.00033(8)	0.00510(9)	0.00299(9)
O(2)	0.00612(14)	0.0087(2)	0.0188(2)	0	0	0.00535(12)
Be	0.0050(3)	0.0050(3)	0.0048(4)	0	0	0.0026(3)
B	0.0050(3)	0.0050(3)	0.0048(4)	0	0	0.0026(3)

Table 5. Selected bond distances (Å) for johnkoivulaite

Cs-O(2)	3.3915(6)
Si-O(1)	1.6041(4)
Si-O(2)	1.6176(6)
Mg-O(1)	2.0878(5)
Mg-Be	2.7336(6)
O(1)-Be	1.5872(4)

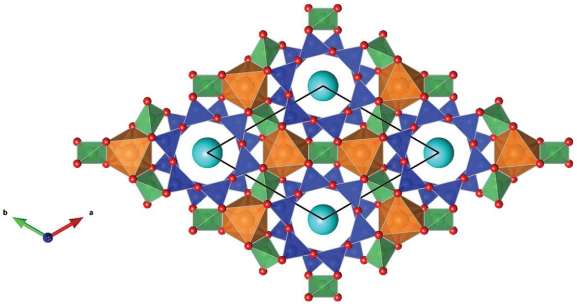

Figure 8. A VESTA 3 (Momma and Izumi 2011) structural diagram of johnkoivulaite down the c-axis. O atoms are shown in red, SiO_4 tetrahedra in blue, MgO_6 octahedra in orange, BeO_4 tetrahedra in green, and Cs atoms in light blue. The black line shows the unit cell.

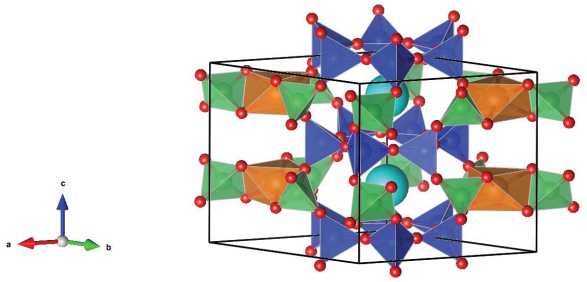

Figure 9. A VESTA 3 (Momma and Izumi 2011) structural diagram of johnkoivulaite almost perpendicular to the *c*-axis showing the stacked Si_6O_{18} rings which define a channel in which the Cs atoms reside. O atoms are shown in red, SiO_4 tetrahedra in blue, MgO_6 octahedra in orange, BeO_4 tetrahedra in green, and Cs atoms in light blue. The black line shows the unit cell.

TABLE 6. Powder diffraction data (*d* in Å) for johnkoivulaite, calculated lines with *I* > 1.5 are listed

I_{obs}	D_{obs}	D_{calc}	I_{calc}	*hkl*
13	8.197	8.2004	5	1 0 0
10	4.743	4.7345	4	1 1 0
17	4.106	4.1002	7	2 0 0
4	3.967	3.9562	2	1 0 2
100	3.272	3.2681	100	1 1 2
82	3.064	3.0995	19	2 1 0
		3.0359	43	2 0 2
85	2.940	2.9317	40	2 1 1
22	2.737	2.7335	14	3 0 0
7	2.559	2.5556	4	2 1 2
18	2.359	2.3673	6	2 2 0
		2.3385	5	3 0 2
27	2.274	2.2744	9	3 1 0
		2.2583	8	0 0 4
22	2.185	2.1773	9	1 0 4
18	2.100	2.0967	9	2 2 2
8	2.039	2.0383	2	1 1 4
		2.0314	2	3 1 2
10	1.8716	1.8668	5	4 0 2
7	1.8461	1.8418	3	3 2 1
17	1.8272	1.8252	4	2 1 4
		1.8148	5	3 1 3
29	1.7939	1.7895	16	4 1 0
40	1.7444	1.7554	2	4 1 1
		1.7410	16	3 0 4
		1.7367	6	3 2 2
24	1.6665	1.6637	14	4 1 2
25	1.6390	1.6340	14	2 2 4
6	1.6016	1.6025	2	3 1 4
		1.5609	2	2 1 5
30	1.5444	1.5497	4	4 2 0
		1.5416	3	5 0 2
		1.5383	7	4 1 3
18	1.4912	1.4898	7	3 3 2
		1.4728	2	5 1 0
13	1.4381	1.4348	9	1 1 6
7	1.4110	1.4133	2	2 0 6
		1.4025	3	4 1 4

IMPLICATIONS

Johnkoivulaite's unusual crystal chemistry

The chemistry of johnkoivulaite is unusual from a geochemical perspective. Two of the elements that occur as major elements in johnkoivulaite, Mg and Cs, are typically concentrated in distinct rock types that are generally geologically unrelated. Cs is usually enriched in granitic and alkali-rich igneous rocks as well as in their associated pegmatites. On the other hand, Mg is usually relatively poor in those rocks but is enriched in rocks that are generally Cs-poor, such as (ultra)mafic/basic rocks and, to an extent, in some marbles. However, this apparent geochemical contradiction might actually provide some clues to the geological genesis of the gem deposits in Mogok. The formation of rubies in the marbles has been linked to the concentration and mobilization of Al and Cr from clay-rich layers in the original limestones, potentially facilitated by the movement of molten salts within the marbles, eventually leading to crystallization of Cr-rich corundum (Garnier et al. 2008). However, given that most of the gem deposits are secondary and there is relatively little exposure of gem-bearing primary host rocks, the specific geological conditions needed to form some of the other gemstones, such as the sapphires, are less well understood. The current thinking by most researchers is that sapphires formed in syenitic pegmatites through interaction with marbles or other metamorphic rocks into which the pegmatites were injected (Thu 2007). The unusual chemistry of johnkoivulaite seems to support the latter part of this hypothesis. This unique chemistry could have been formed by the introduction of Cs from pegmatites, which intruded into marbles or other metamorphic rocks that were enriched in Mg.

TABLE 7. Minerals of the beryl group

	Ideal chemical formula	Symmetry (space group)
Beryl	$Be_3Al_2Si_6O_{18}$	*P6/mmc*
Bazzite	$Be_3Sc_2Si_6O_{18}$	*P6/mmc*
Indialite	$(Mg_2Al)Al_2(AlSi_5)O_{18}$	*P6/mmc*
Ferroindialite	$[(Fe^{2+},Mg)_2Al]Al_2(AlSi_5)O_{18}$	*P6/mmc*
Stoppaniite	$Be_3Fe_2^{3+}Si_6O_{18}{\cdot}H_2O$	*P6/mmc*
Johnkoivulaite	$Cs(Be_2B)Mg_3Si_6O_{18}$	*P6/mmc*
Pezzottaite	$Cs(LiBe_2)Al_2Si_6O_{18}$	*R3c*

Occupancy and hydration of the channel sites in johnkoivulaite

The nearly full occupancy of the 2*a* channel site is another unique aspect of the structure. The implication is that johnkoivulaite must be a relatively dry (water-poor) member of the beryl group. The 2*a* channel sites are separated from each other by a distance of 4.517 Å in johnkoivulaite. If all the 2*a* sites are occupied by Cs^+ ions (ionic radius = 1.88 Å), there is a distance of only 0.757 Å between the Cs^+ ions. This precludes the presence of an H_2O molecule in the 2*b* site, which is between adjacent 2*a* sites. Nonetheless, the FTIR spectra did indicate the presence of H_2O in johnkoivulaite. Given that the occupation of the 2*a* site is only at 96% capacity, it is expected that there should be some limited room for H_2O molecules in the 2*b* site.

On the other hand, most members of the beryl group have well below 50% occupancy of alkali cations at the 2*a* site allowing for the significant occupation of the 2*b* site by H_2O molecules. One major exception to this is pezzottaite, which often has >50% occupancy of the 2*a* site, but never approaches the 2*a* site occupancy of johnkoivulaite. In this regard, johnkoivulaite can be considered a stuffed, comparatively dry beryl group mineral.

ACKNOWLEDGMENTS

We thank two reviewers for their constructive comments and suggestions that have strengthened this manuscript. We also thank Mike Breeding (GIA) and Evan Smith (GIA) for reading the manuscript and providing additional comments and editing for grammar and style. Much gratitude is owed to Associate Editor Fabrizio Nestola and the rest of the editorial staff at *American Mineralogist* as well.

FUNDING

The Bruker D8 Kappa X-ray diffractometer was purchased via an NSF CRIF:MU award to the California Institute of Technology (CHE-0639094) and upgraded with a Dow Next Generation Instrumentation Grant. EPMA analysis was carried out at the Caltech GPS Division Analytical Facility, which is supported, in part, by NSF Grants EAR-0318518 and DMR-0080065. George Rossman's contribution to this work was also supported by NSF Grant EAR-1322082. A portion of this study was funded by the John Jago Trelawney Endowment to the Mineral Sciences Department of the Natural History Museum of Los Angeles County.

REFERENCES CITED

Adams, D.M., and Gardner, I.R. (1974) Single-crystal vibrational spectra of beryl and dioptase. Journal of the Chemical Society, Dalton Transactions, 14, 1502–1505.

Armstrong, J.T. (1995) CITZAF: A package of correction programs for the quantitative electron microbeam X-ray analysis of thick polished materials, thin films, and particles. Microbeam Analysis, 4, 177–200.

Aurisicchio, C., Fioravanti, G., Grubessi, O., and Zanazzi, P.F. (1988) Reappraisal of the crystal chemistry of beryl. American Mineralogist, 73, 826–837.

Aurisicchio, C., Grubessi, O., and Zecchini, P. (1994) Infrared spectroscopy and structural chemistry of the beryl group. Canadian Mineralogist, 32, 55–68.

Brown, G.E., and Mills, B.A. (1986) High-temperature structure and crystal chemistry of hydrous alkali-rich beryl from the Harding pegmatite, Taos County, New Mexico. American Mineralogist, 71, 547–556.

Bruker (2001) SADABS. Bruker AXS Inc., Madison, Wisconsin, U.S.A.
——— (2012) APEX3. Bruker AXS Inc., Madison, Wisconsin, U.S.A.
Fridrichová, J., Bačík, P., Ertl, A., Wildner, M., Dekan, J., and Miglierini, M. (2018) Jahn-Teller distortion of Mn^{3+}-occupied octahedral in red beryl from Utah indicated by optical spectroscopy. Journal of Molecular Structure, 1152, 79–86.
Fritsch, E., and Rossman, G.R. (1988) An update on color in gems. Part 2: Colors involving multiple atoms and color centers. Gems and Gemology, 24, 3–15.
Garnier, V., Giuliani, G., Ohnenstetter, D., Fallick, A.E., Dubessy, J., Banks, D., Vinh, H.Q., Lhomme, T., Maluski, H., Pêcher, A., Bakhsh, K.A., Long, P.V., Trinh, P.T., and Schwarz, D. (2008) Marble-hosted ruby deposits from Central and Southeast Asia: Towards a new genetic model. Ore Geology Reviews, 34, 169–191.
Gübelin, E., and Koivula, J.I. (1986) Photoatlas of Inclusions in Gemstones. ABC Edition, Zurich.
Hagemann, H., Lucken, A., Bill, H., Gysler-Sanz, J., and Stalder, H.A. (1990) Polarized Raman spectra of beryl and bazzite. Physical Chemistry of Minerals, 17, 395–401.
Kim, C.C., Bell, M.I., and McKeown, D.A. (1995) Vibrational analysis of beryl ($Be_3Al_2Si_6O_{18}$) and its constituent ring (Si_6O_{18}). Physica B: Condensed Matter, 205, 193–208.
Lafuente, B., Downs, R.T., Yang, H., and Stone, N. (2015) The power of databases: The RRUFF project. In T. Armbruster and R.M. Danisi, Eds., Highlights in Mineralogical Crystallography, p. 1–30. Berlin, Germany, De Gruyter.
Lambruschi, E., Gatta, G.D., Adamo, I., Bersani, D., Salvioli-Mariani, E., and Lottici, P.P. (2014) Raman and structural comparison between the new gemstone pezzottaite $Cs(Be_2Li)Al_2Si_6O_{18}$ and Cs-beryl. Journal of Raman Spectroscopy, 45, 993–999.
Momma, K., and Izumi, F. (2011) VESTA 3 for three-dimensional visualization of crystal, volumetric and morphology data. Journal of Applied Crystallography, 44, 1272–1276.
Nassau, K., and Wood, D.L. (1968) An examination of red beryl from Utah. American Mineralogist, 53, 801–806.
Palke, A.C., and Hapeman, J. (2019) New find of deep blue aquamarine from Nasarawa State in Nigeria. Gems and Gemology, 55, 437–439.
Searle, M.P., Noble, S.R., Cottle, J.M., Waters, D.J., Mitchell, A.H.G., Hlaing, T., and Horstwood, M.S.A. (2007) Tectonic evolution of the Mogok metamorphic belt, Burma (Myanmar) constrained by U-Th-Pb dating of metamorphic and magmatic rocks. Tectonics, 26, TC3014. DOI: 10.1029/2006TC002083
Taran, M.N., and Rossman, G.R. (2001) Optical spectroscopic study of tuhualite and a re-examination of the beryl, cordierite, and osumilite spectra. American Mineralogist, 86, 973–980.
Thu, K. (2007) The igneous rocks of the Mogok Stone Tract: their distribution, petrography, petrochemistry, sequence, geochronology and economic geology. Ph.D. thesis, Yangon University, Yangon, Myanmar.

Manuscript received September 1, 2020
Manuscript accepted November 25, 2020
Manuscript handled by Fabrizio Nestola

Endnote:

[1]Deposit item AM-21-117785, Online Materials. Deposit items are free to all readers and found on the MSA website, via the specific issue's Table of Contents (go to http://www.minsocam.org/MSA/AmMin/TOC/2021/Nov2021_data/Nov2021_data.html). The CIF has been peer reviewed by our Technical Editors.